Conduit resonance models for long-period seismicity at Galeras volcano (Colombia), during 2004–2010

Óscar E. Cadena [a,*], John J. Sánchez [b]

[a] *Servicio Geológico Colombiano, Observatorio Vulcanológico y Sismológico de Pasto, Calle 27 N.° 9 Este - 25, Barrio La Carolina, Pasto, Colombia*
[b] *Departamento de Geociencias y Medio Ambiente, Facultad de Minas, Universidad Nacional de Colombia-Sede Medellín, Carrera 80 #65-223, Bloque M2, Medellín, Colombia*

ARTICLE INFO

ABSTRACT

This study analyzes the long-period (LP) seismicity of Galeras volcano from the period 2004–2010, based on resonance models of a magma column. In this model an initial disturbance is propagated through the magma column's walls in the form of waves until it reaches a receiver located on the surface. The input parameters for the crust and magma were obtained from previous studies, and the solution of the systems of equations was found using a finite element method. Models for two groups of LP events were found: group G1 associated with the emplacement of the lava domes in 2006 and 2008, and group G2 related to the seismicity preceding the emplacement of these domes. Group G1 is modeled by the resonance of a magma column about 2800 m long with its top near the surface and group G2 is related to a column close to 2000 m in length. The main frequency of initial perturbation differs between the groups. Additionally, the results of this study cast doubt on the effectiveness of location methods of fluid-related seismicity based on amplitude attenuation.

1. Introduction

Galeras volcano (GV) is located in southwestern Colombia, 9 km from Pasto city, capital of the Department of Nariño, with approximately 500,000 people living in its influence area. The GV belongs to Galeras Volcanic Complex (GVC), estimated to be more than 1 million years old (Cepeda, 1986). According to Murcia and Cepeda (1991) the eruptive products of the GVC are mainly composed of lava flows as well as deposits of pyroclastic flows, ash fallout, debris avalanches and lahars. The GVC has produced effusive and explosive eruptions that formed a stratovolcano that suffered two sector collapse events (Calvache, 1990). The GV has an age of ~4500 years. It is the most recent eruptive center of the GVC and has a predominantly andesitic composition, with six eruptive periods (Calvache, 1990; Calvache and Williams, 1997). According to Espinosa (2001) and Cepeda (2020), historically there were 63 documented eruptions between 1535 and 1936. Since the beginning of permanent monitoring of Galeras in 1989 by the Servicio Geológico Colombiano (SGC), through the Observatorio Vulcanológico y Sismológico de Pasto (SGC-OVSP), 21 vulcanian type explosive eruptions have been recorded.

Throughout the history of seismological monitoring, different earthquake types have been recorded in GV, including those related to fracturing of rocky material of the volcanic edifice, called volcano-tectonic (VT) earthquakes and those related to fluid movement inside the volcanic plumbing system or related to ascent of fluids through the volcano conduit. The latter type of seismicity is called long-period (LP) when the source is a transient, and volcanic tremor (TRE) when the source persists in time. The seismicity studied in this work is the LP type, recorded between 2004 and 2010, when two lava domes were emplaced at the base of the main crater, one in 2006 and other in 2008. The lava domes were later destroyed by the eruptions between 2006 and 2010.

Ferrazzini and Aki (1987), Chouet (1986, 1988), Jousset et al. (2003), Sturton and Neuberg (2003, 2006), Neuberg et al. (2006), Smith (2006), among others, have built state of the art models through which it is possible to study LP earthquakes as a consequence of magma or gas movement within a volcanic system. In general, these authors suggest that the resonance of gas-filled crack walls or magma-filled conduits is the source generating most of LP events. In this work we model LP seismicity following the studies mentioned above, as their ideas are applicable to the extrusion stage of the lava domes of 2006 and 2008 at GV.

By varying the length of the magma column in their model, Sturton and Neuberg (2006) observed the existence of "subevents" in synthetic seismograms. These are reflections at the ends of the conduit that are

more appropriately called "echoes", a term that we will use from here-after. Based on this theory, we searched for evidence of echoes within real seismograms in order to estimate the length of the magma column associated with LP events in GV from 2004 to 2010.

The objective of this study is to model the LP earthquake source based on the resonance of magma columns, with an initial disturbance that propagates in the form of waves through the magma column and the conduit walls until it reaches a receiver located on surface. These models are parameterized using pre-existing information from specific studies of the volcano's internal structure and its internal fluid components. The systems of equations were solved using a finite element method and the results are presented as synthetic seismograms which are comparable with real seismograms recorded during the studied period.

This study analyzes the pulses (seismic echoes) in the waveforms of Galeras LP earthquakes and its relationships with the length of the magma column that produce it. The contrast between the synthetic seismograms with real earthquakes is also presented. A model corresponding to the earthquakes associated with the pre-dome stage and another one related to the emplacement of the lava domes are proposed. Finally, a discussion of the results and their possible applications, scope and limitations is presented.

2. The model

This study is carried out in a 2D environment in which we configure the model as the cross-section of a magma-containing conduit surrounded by shallow crustal conditions corresponding to the GVC edifice. The profile passes through a reference seismic station called Cufiño (located 1.9 km northeast of the active cone and 3800 m.a.s.l.) and cuts across the main crater. The conduit, a vertical cylinder opened from the surface down to a certain depth, is modeled as a rectangle with its depth dimension much longer than its width, with a ratio of 100/1. The conduit contains magma from its base to a certain height. Magma is physically modeled by its density, acoustic velocity, and viscosity. Regarding its rheology, we consider it to be a null flow of magma. Somewhere within the magma column, a transient pressure source is located which can last between 0.2 and 1.9 s.

The surrounding crust is modeled as shown in Fig. 1. The model includes: (1) A 6 km wide by 5 km tall rectangular-shaped polygon of linear and isotropic elastic material; (2) Three rectangle-shaped layers of 0.5 km width located at the sides and base of the first structure (These
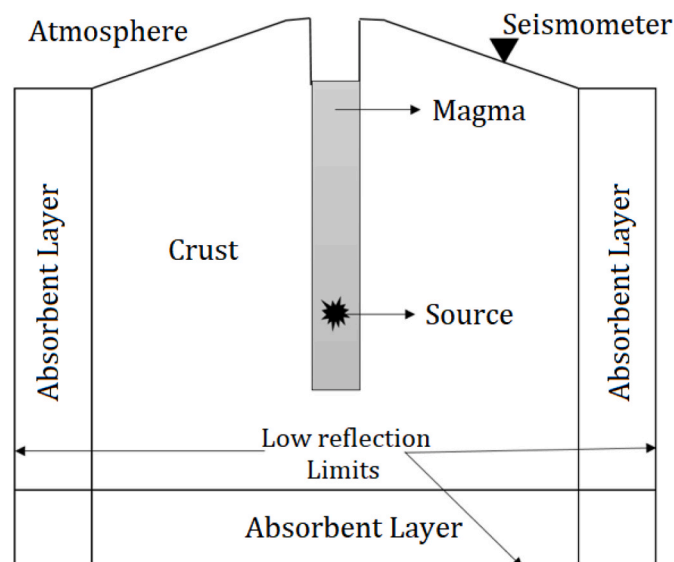
Fig. 1. General scheme of the elements that form the basis of the conduit model for the GV region. Some elements of the graph have been exaggerated for better visualization.

layers correspond to virtual domains in order to simulate both lateral and deep unbounded or infinite domains. The layers are Perfect Matched Layer (PML) type (COMSOL Multiphysics, 2019) and act by absorbing the energy of waves fronts coming from the source. They avoid unwanted reflections that return energy back to the system because we are not interested in the solutions far away from the source, and (3) A low-reflection interface surrounding the absorbing layers to emphasize the characteristic of no lateral or depth reflections. This boundary condition takes the material data from the adjacent domain in an attempt to create a perfect impedance match for both pressure waves and shear waves (Structural Mechanics Module, 2018).

The results of the models are shown in synthetic seismograms at a location corresponding to Cufiño station.

2.1. Elastic parameterization of the GV

Torres (2012) obtained a 3D model of the internal structure of GV using a passive local seismic velocity tomography. The data used by Torres (2012) corresponds to the period of seismic activity from 1989 to 2009, covering most of the period analyzed in the present study (2004–2010). Torres (2012) suggests a vertical structure with brittle behavior that could be associated with old intrusive or volcanic rocks through which new magma ascends, indicating the presence of a conduit or currently active faults. The 3D P-wave velocity model estimates the variation in density and Poisson's ratio using the specific regression settings of Brocher (2005) for each parameter, and also computes the shear and bulk moduli. Obtained values agreed with the results of gravimetric studies on the GV (Ortega, 2014).

In order to obtain adequate values to characterize the region, the elastic parameter values found by Torres (2012) for specified cross-section of interest, were averaged (Table 1).

Where Vp, Vs and Vp/Vs, correspond to the P and S-wave velocities and their ratio, respectively; ρ, ν, μ, K and E are: density, Poisson's ratio, shear modulus, bulk modulus and Young's modulus, respectively.

2.2. Properties of Galeras magma

2.2.1. Major oxides

The physical properties of magma are closely related to its chemical composition, which is usually expressed in terms of its major oxide content. The SGC performed the analysis of samples collected after the GV eruption on January 17, 2008; the techniques applied were: Atomic absorption-flame and inductively coupled plasma optical emission spectroscopy (ICP-OES) (INGEOMINAS, 2008c) and Bain et al. (2019) obtained results through EPMA (Electron Probe Micro-Analyzer) analysis on both microlites and groundmass glass. Table 2 summarizes the results from both studies.

2.2.2. Crystal fraction

Stix et al. (1997) used a value of 35 vol% for their calculations in studies related to the Galeras eruption period 1992–1993. In contrast, Pulgarín (2006), who studied bombs from the July 12, 2006 eruption, mentions that the macroscopically analyzed rocks are porphyritic in texture, have 70 vol% of matrix rich in glass, 28 vol% of plagioclase crystals and 2 vol% of mafic crystals (pyroxenes). Another analysis carried out by INGEOMINAS, in which pyroclastic fragments

Table 1
Elastic parameter values used for this study, computed from Torres (2012).

DEPTH (KM)	VP (KM/S)	VS (KM/S)	VP/VS	P(KG/M³)	N	M(N/M²)	K(N/M²)	E (N/M²)
0–6	3.3	1.78	1.85	2278	0.29	1.4×10^{10}	1.5×10^{11}	1.9×10^{11}

Table 2

Mayor oxides values resulting from studies of INGEOMINAS (2008c) on samples from material expelled by the GV between 2006 and 2010 and those of Bain et al., (2019) for samples erupted between 2004 and 2010. First row: whole-rock values for bombs and blocks. Second and third rows: mean values for microlite samples and groundmass glass in bombs, respectively.

Reference	SIO_2	AL_2O_3	FEO*	MGO	CAO	TIO_2	NA_2O	K_2O	MNO	P_2O_5	SRO
INGEOMINAS (2008c)	58.58	17.38	9.68	3.39	6.69	0.76	3.67	1.57	0.10	0.36	–
Bain et al., (2019)-plagioclase microlites	56.17	26.65	2.67	0.08	9.71	–	5.67	0.67	0.01	–	0.12
Bain et al., (2019)-groundmass glass	76.23	11.86	1.90	0.15	0.60	0.54	3.64	4.81	0.03	0.06	–

corresponding to the January 17, 2008 eruption were studied, indicates that the phenocryst content is between 30 and 40 vol%, mainly of plagioclase (INGEOMINAS, 2008a). The most recent study by Bain et al. (2019) finds crystal content values between 16 and 55 vol%, with an average of 38 vol%. Taking into account these references, a representative range for crystal content between 35 and 40 vol% used for the present study.

2.2.3. Temperature

Stix et al. (1997) used temperature values found by Goff et al. (1994) and Calvache and Williams (1997), based on thermometry of dome samples, which yielded temperatures of $1000 \pm 50\ °C$ and 900–945 °C respectively. In the studies of Bain et al. (2019) a value of 980 °C was used for viscosity calculations and other magma properties, a value that is adopted for the present work.

2.2.4. H_2O content

The first calculations of the percentage of water content in the GV magma, correspond to whole-rock chemical analyses with variations between 0 and 2 wt% (Stix et al.,1993). Calvache and Williams (1997) and Stix et al. (1997) use these values to perform calculations in their respective works. Recently, Bain et al. (2019) founds values between 0.05 and 1.01 wt% in matrix glass samples, and values larger than 0.4 wt % for bomb samples. A range of values representative for the GV magma between 0.5 and 1.5 wt% water content, is used in the present work.

2.2.5. Density, viscosity and acoustic velocity

We implemented one-dimensional models of magma flow in conduits using the Conflow (Mastin, 2002) and Confort15 (Campagnola et al., 2016) computer programs to estimate ranges of density, viscosity and acoustic velocity of GV magma (Table 3). The input values, results and analysis are available within "Physical properties of Galeras magma - Conflow and Confort15.docx", online supplementary material.

2.3. Conduit diameter

In this study, the volcanic conduit is represented with a constant-diameter geometry. Smith (2006) assumed diameters of 30 or 50 m at the Soufriere Hills volcano. Sturton and Neuberg (2006) also used a constant diameter of 30 m as the conduit width and mentioned that based on the work of Sturton and Neuberg (2003), possible variations in conduit diameter between 30 and 90 m do not induce significant differences in the results. Harnett et al. (2018) using discrete elements to model the emplacement and collapse of lava domes, used a diameter of 20 m. Using photographs of the Galeras dome in 1991, we estimate diameters in the range 55–104 m; in contrast, field measurements in October 1991, indicated a diameter in the range 80–100 m (Gómez

Table 3

Density, acoustic speed and viscosity depending on the water contents in the GV magma.

h_2O (WT%)	DENSITY (KG/M^3)	ACOUSTIC SPEED (M/S)	VISCOSITY (pA.S)
0.5	2509	2485	2.00×10^6
1.0	2472	2254	5.01×10^5
1.5	2430	2093	2.00×10^5

et al., 2006). We infer that the diameter of the conduit must be smaller than any of the mentioned values. Based on the above, we assume a constant diameter of 30 m for GV's conduit.

2.4. Topographic approach

Although authors such as Neuberg et al. (2000), Neuberg et al. (2006) and Jousset et al. (2004) demonstrated that the inclusion of topography has the effect of adding dispersion in the seismograms, in the present work such dispersive effects are not taken into account because the main goal is to reproduce the general characteristics of the waveforms and spectral content of the LP seismicity at a single station. Therefore, the detailed topography of the area is not included in our conduit model. However, a slope that simulates the hillsides of the volcano has been included in order to locate the virtual seismometer in a similar position of to real seismometer (Cufiño station).

2.5. Finite element method (FEM)

The model covers two domains: solid and fluid, that each control wave propagation in a different way, therefore, from specific initial conditions, the equations involved in the system must provide the solution of the pressure field within the fluid and the displacement field in the solid medium, including the respective interaction between both domains at their contact interfaces.

The solid domain is controlled by equation:

$$(\lambda + \mu)\nabla(\nabla.\boldsymbol{u}(\boldsymbol{x},t)) + \mu\nabla^2\boldsymbol{u}(\boldsymbol{x},t) = \rho_s\frac{\partial^2\boldsymbol{u}(\boldsymbol{x},t)}{\partial t^2} \tag{1}$$

which corresponds to the general seismic wave equation, and it is solved for the displacements $\boldsymbol{u}(x,t)$ in the x and y dimensions, where λ and μ correspond to the elastic Lamé constants and ρ_s is the average density of the crust.

Wave propagation in the fluid domain is controlled by:

$$\frac{1}{\rho_f c^2}\frac{\partial^2 P}{\partial t^2} + \nabla.\left(-\frac{1}{\rho_f}(\nabla P - q_d)\right) = Q_m \tag{2}$$

where P corresponds to the pressure field $P(x,t)$, ρ_f is the fluid average density, c the acoustic velocity and Q_m and q_d represent the source transient. On the other hand, the intrinsic attenuation is controlled by the fluid viscosity which is introduced to the system of equations by the Rayleigh attenuation coefficient (Clay et al., 1977).

The finite element method is part of the set of numerical methods that offers approximate solutions to problems described through differential equations that are solved on specific geometries. Basically, it requires concrete knowledge of the constitutive and time evolution equations. One of the most sensitive factors within this solution method is the size of the elements used to discretize the domains; one of the advantages of the program that was used (COMSOL Multiphysics, 5.5), is to generate an appropriate meshing, taking into account the shortest wavelengths of the model, the highest wave velocity value and the smallest mesh element (COMSOL Multiphysics, 2019), based on the physics of the problem. The maximum element size lmax that is directly related to the smallest wavelength varies in the range:

$$\frac{c_{min}}{1.5\,f_{max}} \quad to \quad \frac{c_{min}}{2\,f_{max}} \tag{3}$$

where fmax is the maximum frequency and cmin corresponds to the lowest velocity value in the model. In this way, the meshing included 2441 elements with a minimum quality of 0.4815.

The synthetic seismograms have been configured with a sampling rate equal to that of the real seismograms, $\Delta t = 0.01$ s, which makes it possible to study frequencies up to 50 Hz.

3. Results

First of all, to identify possible seismic echoes in real seismograms, we manually inspected LP earthquakes in the period 2004–2010. As result of this review, we found that most of them showing clear pulses within their waveforms (Fig. 2).

3.1. Verification of seismic echo in real seismograms

In a set of 267 signals recorded at Cufiño station it was possible to measure the time between pulses (Table 4). These earthquakes were chosen, taking into account the pre-dome and emplacement stages of the 2006 and 2008 domes in GV. Cadena (2021), proposes the existence of two groups of families of earthquakes that share spectral characteristics. The earthquakes of these groups are distributed in time as follows: group G1 associated with the emplacement of the domes and group G2 related to pre-dome stages.

3.2. Magma column length based on seismic echoes

Assuming that most of the energy released at the source travels along the magma column and that energy is transmitted in greater proportion through the top and base of the column, the pulses of the seismograms represent the energy that escapes from the conduit through its ends and reaches the seismometer with pulses of higher amplitude energy. In that case, the time lapse between one pulse and the next, corresponds to the travel time of a pulse in the top-base-top trajectory, and therefore, the length of the column would be determined by:

$$L_m = \frac{ct}{2} \tag{4}$$

where c is the acoustic velocity of the fluid and t is the time between successive pulses.

Finally, based on the inter-pulse time readings (Table 4), the acoustic velocity values recorded in Table 3 and equation (2), a matrix of probable values for magma column length was constructed (Table 5).

According to results of Table 5, it is possible to constrain the length of the magma column for the generation of LP earthquakes to an interval between 1925 m and 2522 m, taking into account the error values.

Table 4
Results of measuring seismic echo intervals.

pARAMETER	G1-2006	G2-2006	G2-2008
NUMBER OF EARTHQUAKES	75	73	119
MEAN (S)	1.99	1.87	1.98
STANDARD ERROR (S)	0.04	0.03	0.09
STANDARD DEVIATION (S)	0.35	0.23	0.96

Table 5
Possible magma column lengths. Values in bold correspond to the extreme values in the matrix.

ACOUSTIC SPEED (M/S)	G1-2006 (M)	G2-2006 (M)	G2-2008 (M)
2485	**2472 ± 50**	2320 ± 34	2459 ± 109
2254	2242 ± 46	2105 ± 31	2231 ± 99
2093	2082 ± 42	**1954 ± 29**	2071 ± 92

3.3. Synthetic seismograms

Fig. 3 and Table 6 describe the model for the resonant conduit for LP that correspond to synthetic seismograms.
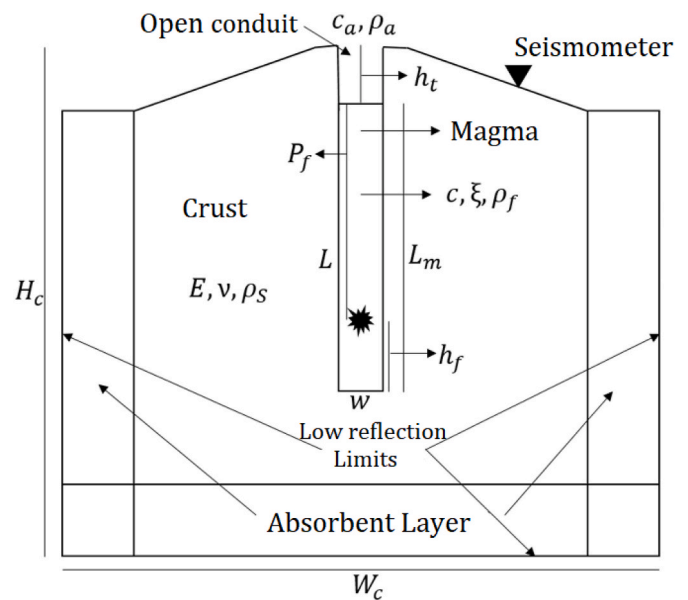
Fig. 3. Model to generate synthetic seismograms. (Scheme is not presented at scale to better visualize the small features.)
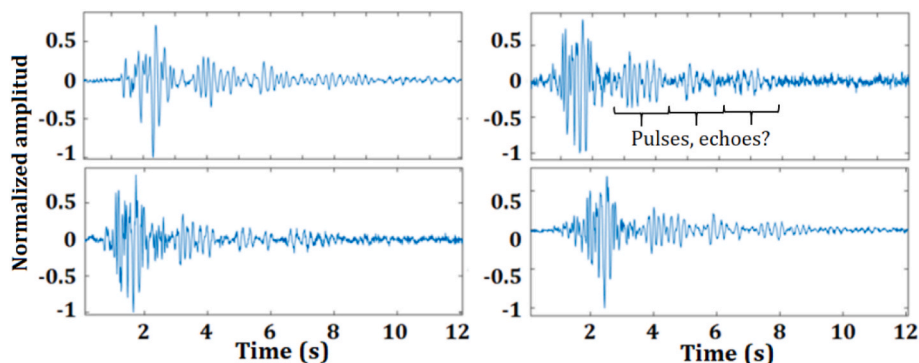
Fig. 2. Examples of real seismograms recorded by vertical component of Cufiño station during 2004–2010.

Table 6

Parameters used in the schema in Fig. 3. Fields that contain the word "variable" imply that their corresponding value can be modified.

Parameter	Description	Value, units
H_c	Crust thickness	5000 m
W_c	Crust width	7000 m
W_{abs}	Absorbent layer width	500 m
S_x	Sismometer position x	1900 m
S_y	Sismometer position y	−395 m
Δt	Sampling rate	0.01 s
L	Conduit length	variable (m)
L_m	Magma column length	Variable (m)
w	Conduit width	30 m
P_f	Source depth relative to top of conduit	variable (m)
h_f	Height of the source with respect to the base of the conduit	variable (m)
f	Source frequency	Variable (Hz)
h_T	Depth of the top of the conduit relative to the top	variable (m)
c	Acoustic speed of fluid (magma)	variable (m/s)
c_a	Acoustic air speed	343 m/s
E	Young's modulus	1.9×10^{11} N/m^2
ν	Poisson's ratio	0.29
ξ	Magma viscosity	variable (Pa*s)
ρ_s	Solid density (crust)	2278 kg/m^3
ρ_f	Fluid density (magma)	variable (kg/m^3)
ρ_a	Air density	1.2 kg/m^3
g	Gravity value	9.8 m/s^2

3.3.1. Model selection

Two hundred twenty-five different models were tested. Nine were selected and their results show spectral similarities with earthquakes of groups G1 and G2 recorded in the period 2004–2010 (Cadena, 2021). The file "Synthetic seismograms spectral parameters.xlsx", available in the online supplementary material, shows the spectral characteristics obtained with these nine models. Each graph corresponds to a parameter of their corresponding synthetic seismograms. Based on these results two groups of synthetic earthquakes are proposed, G1S containing models 313, 325, 326, 402, 405 and 407, and G2S with models 315, 330 and 350. The selection criterion of these sets was the similarity in the values of their spectral characteristics. Additionally, the proposed G1S and G2S are related to the spectral characteristics of groups G1 and G2 of real earthquakes found by Cadena (2021).

Restrictions to spectral criteria must be added considering the time interval between pulses in each of the nine selected synthetic seismograms (Table 7). This constrains the conduit length in the models.

In order to limit the number of models it is necessary to constrain the time interval between pulses considering the values from real seismograms (Table 4), where an interval between 1.84 s and 2.07 s was defined. From nine selected models, only four remained in the observed interval: 325 and 326 from group GS1 and 330 and 351 from group GS2.

Another factor to constrain the models considers the H$_2$O content in magma, given that for a mixture with 1.5 wt % of water, both density and acoustic velocity vary rapidly from surface to about 2400 m depth

(Figure A2 within "Physical properties of Galeras magma - Conflow and Confort15.docx", online supplementary material); then, in a conduit of 3000 m measured from top, only the deepest 600 m could contain magma with relatively stable values in these physical properties. This prohibits the possibility of adopting them as realistic models based on observations of seismic echoes in real seismograms. Thus, model 325, which includes 1.5 wt % H$_2$O, was discarded.

An additional restriction considers the a priori assumption that the exciting source of this seismicity is near the conduit base, given that in the context of volcanic activity within the studied period, the characteristics of this activity imply magma input from a certain depth towards the surface through a conduit. At the conduit base pressure fluctuations would arise due to possible variations in the conduit geometry or instabilities in the magma flow (Julian, 1994). Considering the above, model 351, whose source was located 1000 m above the base of the conduit, was discarded.

The nine initially selected models were reduced to two, whose main characteristics are listed in Table 8.

3.4. Model 326 of G1S group

Fig. 4 shows the waveforms and spectra of the *x* (horizontal) and *y* (vertical) components of the synthetic signal for model 326. In the 20 s of recording, pulsatile features are observed. Their spectra contain frequencies in the expected range for real earthquakes of group G1 (Cadena, 2021), with high amplitude energy below 3.8 Hz in *y* component. Fig. 5 show velocity field snapshots obtained with 326 model.

Frames **a** and **b**, which correspond to times 0.47 s and 0.82 s, show waves that arrive at the seismometer traveling directly through the crust, from a zone close to the source. In fact, in **b** we observed the pressure transient keeping its upward travel through the conduit, without having yet reached its top. Frames **c, d, e** and **f**, and their corresponding time stamps in Fig. 4 correspond to the arrival of compressional waves that leave the conduit at its top and reach the seismometer traveling through the shallowest part of the crust.

3.5. Model 330 of G2S group

Fig. 6 shows the pulsating characteristics of the seismograms, more accentuated in the *y* component. Their spectra are wider compared to those of the synthetic seismogram of G1S group, since energy up to 16

Table 8

Main characteristics of models for the G1S and G2S groups.

	G1S	G2S
ID	326	330
h_2o (wt%)	1	1
l (m)	3000	3000
l_m (m)	1960	1960
ρ_f (kg/m^3)	2472	2472
c (m/s)	2254	2254
ξ (Pa.s)	2.51×10^6	2.51×10^6
f_0 (Hz)	4	8
h_f (m)	300	200

Table 7

Time intervals measured for the five pulses of each synthetic seismogram, predicted after the first wave packet. The last row shows the average of the four intervals.

INTERVAL (S)	gS1						gS2		
ID	313	325	326	402	405	407	315	330	351
INTERVAL.1	2.58	1.93	1.84	2.30	2.16	2.16	2.38	1.83	1.83
INTERVAL.2	2.53	1.93	1.83	2.32	2.46	2.45	2.52	1.83	1.85
INTERVAL.3	2.55	1.94	1.83	2.31	2.19	2.44	2.37	1.84	1.84
INTERVAL.4	2.34	1.92	1.84	2.32	2.44	2.48	2.51	1.87	1.84
AVERAGE	2.50	1.93	1.84	2.31	2.31	2.38	2.45	1.84	1.84

Fig. 4. Waveforms and spectra of synthetic seismogram generated with 326 model (GS1).
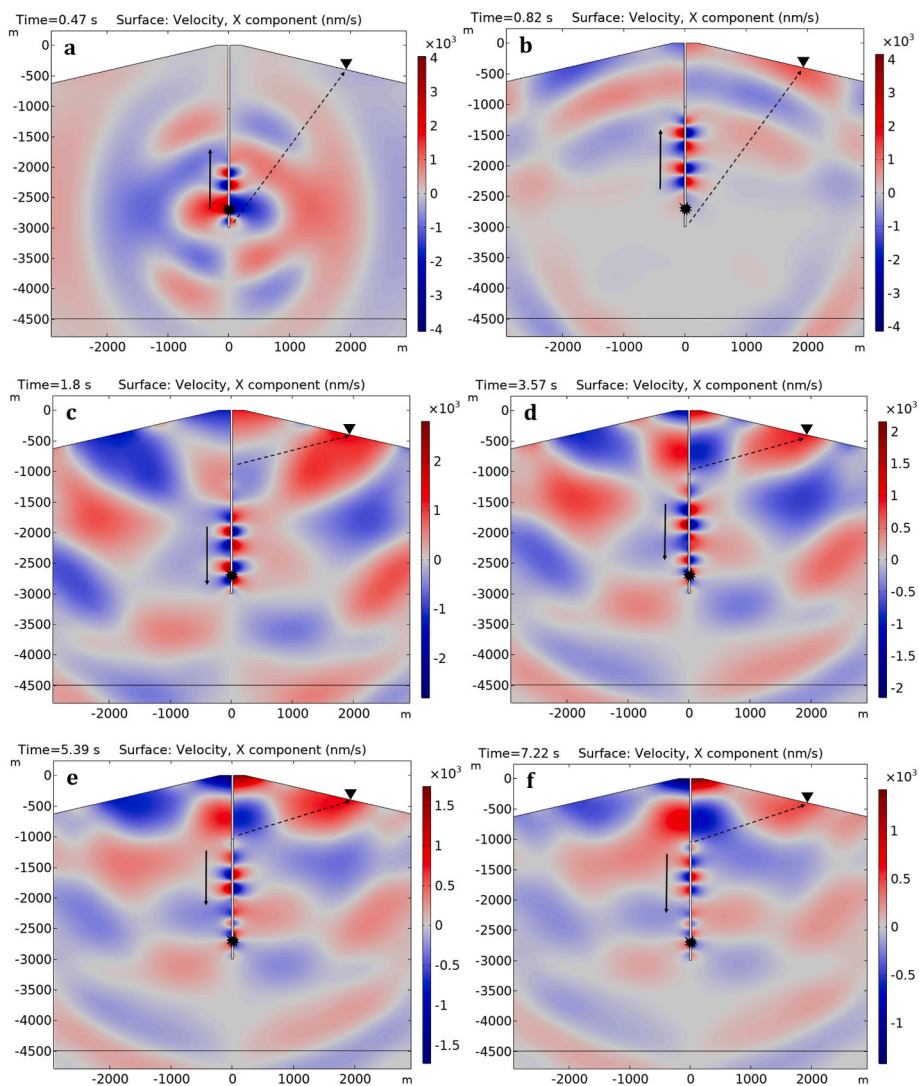
Fig. 5. Frames of speed-field for specific moments (*x* component) of 326 model. Each panel, a-f, corresponds to one of the timestamps in Fig. 4. The black solid vertical arrows represent the direction of the pulse while it travels within the magma column, and the dashed arrow shows the trajectory of each disturbance to the virtual seismometer, outside the conduit. Note that the scale to the right of the figure is not the same for all frames.

Hz is observed in both components, with a dominant band between 4.8 and 7.5 Hz and a subordinate one between 9 and 11.5 Hz, in the y component.

Similarly, frame **a** in Fig. 7 shows the instantaneous configuration of the velocity field after the arrival of direct waves traveling through the crust from a zone near the source. The other frames show compressional waves arriving at the seismometer from the top of the conduit.

3.5.1. Contextualization and complementary physical considerations

Modelling results show an adequate fit to observed signals. However,
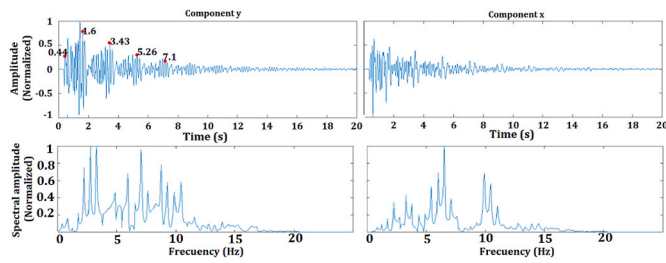
Fig. 6. Waveforms and spectra of synthetic seismogram generated by the 330 model.

these results raise the next questions that could be partially solved by adjusting some model parameters *a posteriori,* based on specific observations of volcanic activity during the period studied.

3.6. Considerations for 326 model - G1S

a. Since the real earthquakes of group G1 were recorded during the dome extrusion (Cadena, 2021), implying that the top of the magma column is about 150 m below the top of the volcano, the validity of model 326 - G1S must be tested by locating the top of magma column at a shallower depth than initially proposed.

b. The average time interval between pulses of the real earthquakes of G1 group is 1.99 ± 0.04 s, while in model 326 it is 1.83 s, which implies the need to increase the length of the magma column in the model.

c. It is reasonable to think that the source is located at the base of the conduit, which is the place where material enters the magma column, therefore, the source should be brought closer to the base of the conduit.

d. A final adjustment considers the envelope of the pulses in the synthetic seismograms, since the number of synthetic oscillations is smaller than observed in the pulses of real seismograms.

The considerations in **a, b** and **c**, were solved with small modifications in the model, however, the observation in item **d** needs a redefinition of the pressure transient.

3.7. Redefinition of the pressure transient

The models tested up to this point assume a source which acts in a transient manner, restricting the definition of "transient" (in this study) to the application of a single pulse represented by a Ricker-type wavelet with amplitude *A* described for.

$A = (1 - 2\pi^2 f^2 (t - t_0)^2) e^{-\pi^2 f^2 (t - t_0)^2}$ where *f* is the frequency and *t* the time. This results in synthetic seismograms with few oscillations per
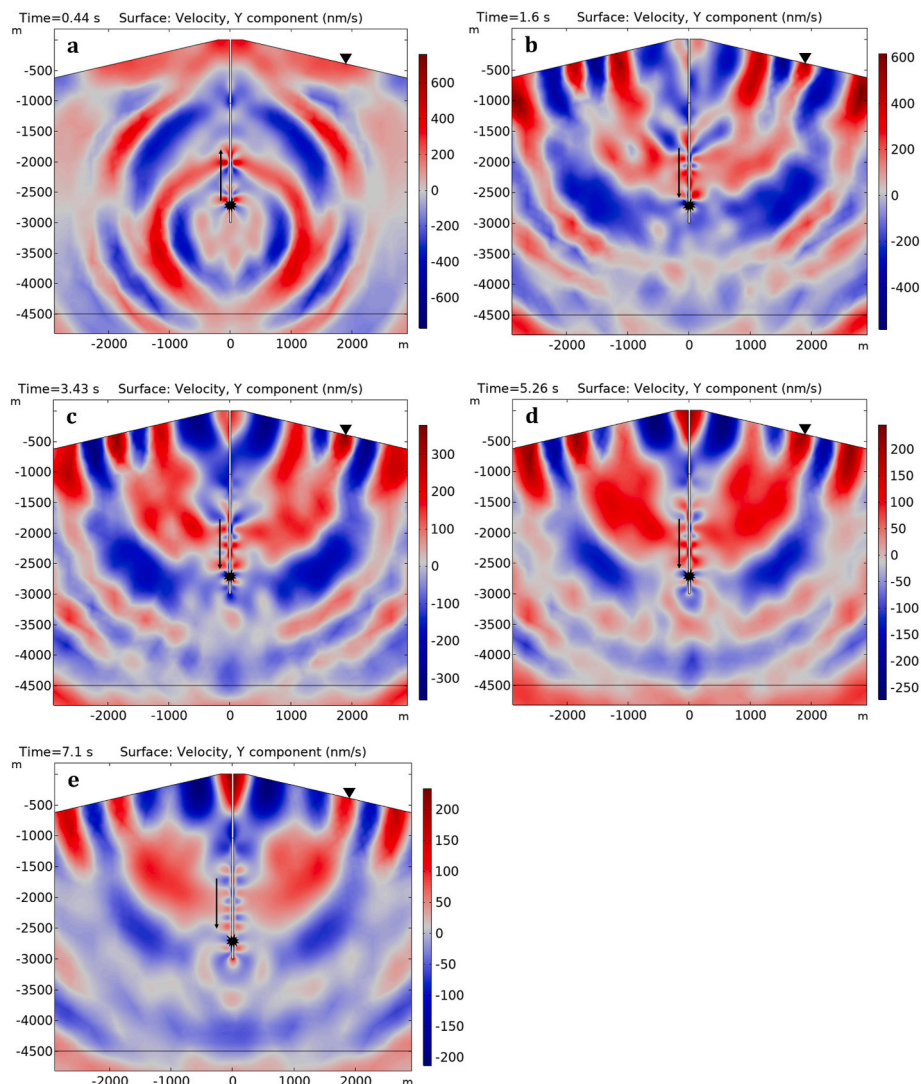
Fig. 7. Model 330 frames for speed-field specific moments (vertical component - *y*). Conventions as in Fig. 5.

pulse (Fig. 4), in contrast to what is observed in most real seismograms (Fig. 8).

In order to include this correction, the "transient" is redefined, allowing the application of a complex pulse formed by several oscillations represented by a chain of Ricker wavelets (Fig. 9 - left). Fig. 9 (center) shows synthetic seismograms resulting from application of two different source waveforms, including three and six peaks. Note that as more oscillations are included in the source pulse, the spectrum is affected by a slight shortening of the bandwidth.

3.8. Considerations for 330 model - G2S

Given the considerations for the real seismicity of G1 group and assuming that the depth of the base of the conduit remains constant throughout the studied period (2004–2010), then:

a) Model 330 of the G2S group should be modified such that the depth of its magma column base matches that of model 326-G1S.
b) The time interval between pulses measured in the real G2 seismograms was 1.87 ± 0.03 s and the one measured in the synthetics was 1.83 s, so it does not requires applying an adjustment to the column length.
c) In the same way as for model 326-G1S, a source as close as possible to the base of the conduit is assumed.
d) The real seismograms of the G2 group of seismicity (Cadena, 2021) do not show pulses with numerous oscillations, therefore, it is not necessary to use multiple wavelets in the source function.

3.8.1. Real vs. synthetic seismograms - specific cases

The 326A-G1S model was generated from the 326-G1S model which was modified based on considerations described below. Similarly, two new models that starts from 330-G2S are proposed and they will be called 330A-G2S and 330B-GS2. The latter includes small differences in source function frequency and source depth. The main characteristics of these models are shown in Table 9. Finally, in order to make a qualitative comparison of the synthetic seismograms with real seismograms, we select earthquakes corresponding to the phase of construction of the domes in 2006 and 2008 and others recorded before the emplacement of the domes. For this qualitative comparison, noise composed of random amplitudes between 2 and 4% of the maximum amplitude was added in the synthetic seismogram, of course, the energetic contribution of this noise is almost imperceptible in the spectrum.
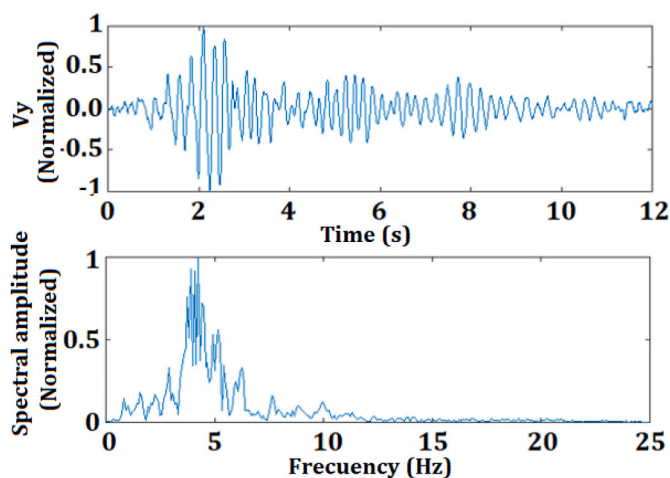
Fig. 8. Real seismogram of G1 group where several oscillations are observed in each pulse. Below is the frequency spectrum.

3.9. Comparison with real earthquakes of G1 group, 2006 and 2008 domes

The source function was configured with seven equally-spaced wavelets for a perturbation time of 1.9 s. Note that in this model the magma column almost reaches the surface, this is in agreement with the fact that the real earthquakes of the G1 group were recorded during the emplacement of the lava domes at the base of the main crater. Fig. 10 shows the comparison between the synthetic seismogram of model 326A-G1S with actual seismograms recorded in February 2006, October and November 2008, which correspond to periods of lava dome emplacement at the surface.

3.10. Comparison with actual earthquakes of G2 group, pre-dome stages of 2006 and 2008

In this case, a source composed of a simple Ricker-type wavelet of 8 Hz was used for comparison with an earthquake of 2005 and one of 10 Hz for the comparisons with an earthquake of 2008, which implies source disturbance times between 0.25 and 0.3 s; additionally, for the comparison with the earthquake of 2008, we used a source location of 350 m above the base of the conduit.

Fig. 11 shows the comparison of the synthetic seismograms resulting from models 330A and 330B, with actual earthquakes recorded in September 2005 and January 2008, months before of the emplacement of the domes of 2006 and 2008 respectively, the actual earthquakes correspond to the group labeled as G2 in Cadena (2021).

4. Discussion

4.1. Models parameterization

This research raises the possibility of applying models in which seismic waves within magma conduits can be used for studying the origin of LP events associated with the intrusion and emplacement of lava domes.

The use of long magma columns inside conduits to explain LP seismicity comes from the works of Sturton and Neuberg (2003, 2006) and Smith (2006), and its application in the GV is supported by studies of its internal structure. Torres (2012), Londoño and Ospina (2008), Carcolé et al. (2006), Vargas et al. (2006), Sanchez et al. (2005) and Moncayo (2004), through different techniques propose anomalies that they interpret as possible elongated structures and magmatic reservoirs up to 9 km depth.

Pulses observed within LP waveforms are analyzed using synthetic signals in order to model reflections of the wavefronts at the top and base of the magmatic conduit. Those pulses are the basis of the hypothesis that we raise and verify through the synthesis of seismograms using models parameterized by information of previous investigations related to the structure of GV and the composition of its magma.

These models require some simplifications, one of which implies that the physical magma properties in the models are assumed to be constant with depth and width. It is known that in reality the properties of the magma inside the conduit vary, both, vertically and horizontally (Collier and Neuberg, 2006), however, Smith (2006) studied models in which the magma properties are a function of the conduit depth, resulting in synthetic seismograms more complex and less similar to the real ones.

The use of Conflow and Confort15 programs (Mastin, 2002; Campagnola et al., 2016) to estimate the physical magma properties, under certain conditions of crystals, water and oxide content, suggested suitable ranges for the model parameterization. Conflow and Confort15 show the depth-dependent pressure, density, acoustic speed and viscosity for Galeras magmas with 37.5% crystallinity and reasonable water contents in the range 0.5–1.5 wt% (Bain, et al., 2019, Calvache and Williams, 1997; Stix et al., 1997; Calvache, 1990). There is a strong dependence of density and acoustic speed on water contents (view
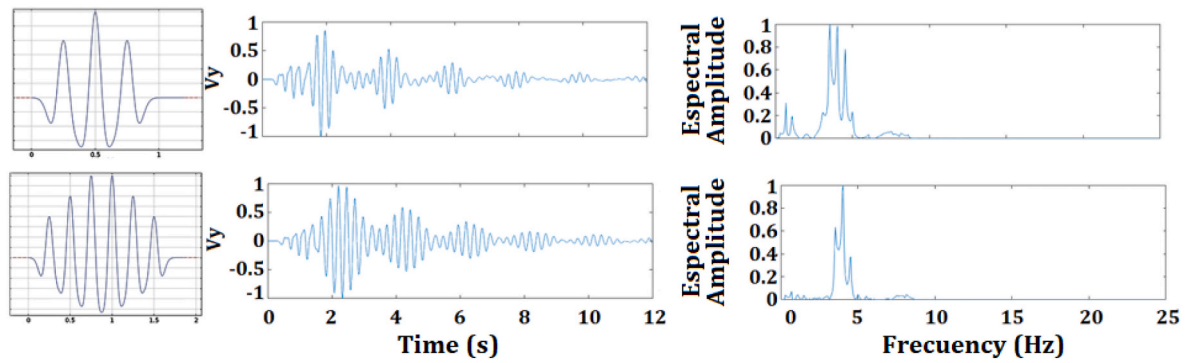
Fig. 9. Synthetic seismograms generated with different types of transients. Left: waveform of applied source. Center: computed seismogram. Right: frequency spectrum.

Table 9
Main characteristics of models for the G1S and G2S groups.

	G1S	G2S
ID	326A	330A–330B
h_2o (wt%)	1	1
l (m)	2950	3000
l_m (m)	2800	1960
ρ_f (kg/m^3)	2472	2472
c (m/s)	2254	2254
ξ (Pa.s)	2.51×10^6	2.51×10^6
f_0 (Hz)	5	8–10
h_f (m)	400	200–350

supplementary material). A constant acoustic speed of 2093 m/s for 1.5 wt% water content is only achieved roughly below 2300 m depth. If the water average content increase beyond the values shown/used, acoustic speed would only be constant at a much greater depth, which would be incompatible with the observations of times lapses between echoes in actual seismograms. A much longer magma column length (as required for higher water content) would not agree with the expected dimensions of the volcanic pipe from other studies.

4.2. Seismic echoes

The pulses observation in the waveforms of actual LP earthquakes recorded between 2004 and 2010 (Fig. 2) suggested, "a priori", the
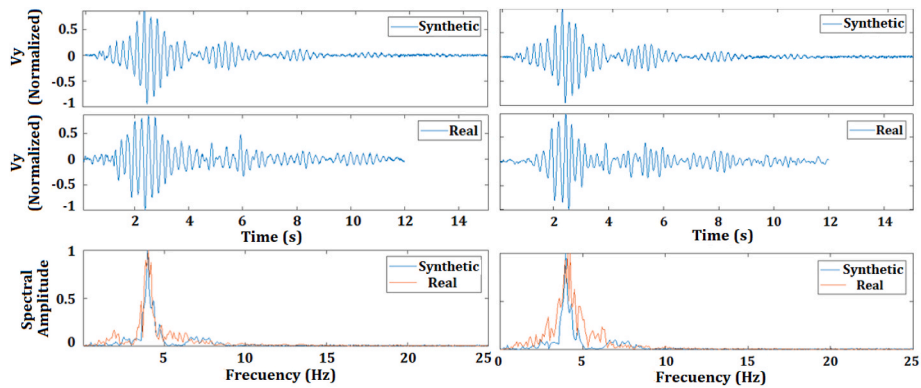
Fig. 10. Comparison of vertical component (*y*) of the synthetic seismogram of model 326A-G1S, with the same component of actual seismograms recorded: February 2, 2006 (left) and November 3, 2008 (right). The computed spectra for each case are also displayed. Note the recreation of the pulsatile characteristics of actual seismogram and the good fit between the corresponding spectral bands.
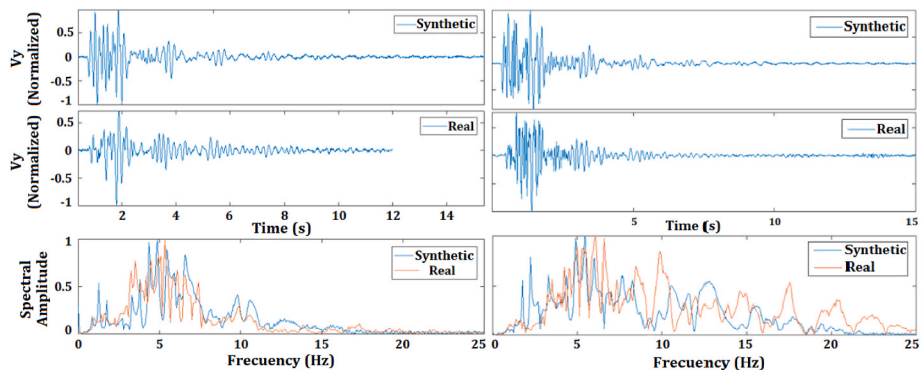
Fig. 11. Comparison of the vertical component (*y*) of the synthetic seismograms of 330A-G2S (left) and 330B-G2S (right) models, with the same component of the actual seismograms recorded on September 13, 2005 (left) and January 17, 2008 (right), respectively.

possibility that these pulses were originated by wavefronts reflections at the ends of a magma column (echoes). The analysis of synthetic seismograms supports this hypothesis showing that the complexity of the LP waveforms is due to the contribution of different wave trains: (1) direct waves from the source to receiver, whose trajectories are quasi-direct through the crust; (2) acoustic and interface waves that leave the column at its top; (3) acoustic and interface waves reflected at the base and returning to the surface traveling through the magma column to leave it at its top; and (4) acoustic and interface waves that leave the column at the base and travel directly through the crust to the receiver (Figs. 4–7). Depending on the length of the magma column, these wave trains may be far enough apart to distinguish them.

The estimation of the length of the magma column from time lapses between pulses and average acoustic velocity of the magma, using a simple equation (Eq. (2)), yielded reasonable results, both in real and synthetic seismograms. The dispersive effects of the interface waves (Ferrazzini and Aki, 1987) were not taken into account, considering that this aspect is beyond the scope of this study.

4.3. LP seismicity models for Galeras

This study establishes a connection between the periods of intrusion and emplacement of lava domes with actual earthquakes in groups G2 and G1, respectively by using synthetic seismograms associated with models of each group. The results suggest an approximately 3000 m conduit long with a magma column of 2800 m and a source frequency of 5 Hz for the G1S group, and a column length of 1960 m with a frequency of 8–10 Hz for the G2S group. These results are consistent with the observations of the lava domes on surface (INGEOMINAS, 2006, INGEOMINAS, 2008b) accompanied by seismicity of G1 group and the record of earthquakes of G2 group when the magma had not yet reached the surface. The above is also supported taking into account that the spectral and waveform characteristics of the synthetic seismograms of G1S and G2S groups show great similarity with those corresponding to real seismograms of G1 and G2 groups (Figs. 10 and 11).

These results suggest that is possible to use this method to estimate the magma column length during a future intrusion and lava dome process.

4.4. Source function

The source function was included by one or several Ricker-type wavelets that represent transient pressure changes near the magma column base. This source function could be related to instabilities of the magma flow. According to Julian (1994) these instabilities could be related to the way in which magma is supplied in the conduit or irregularities in the conduit geometry, for example, "necks" could change the pressure drastically.

Another important consideration is related to the differences between the source functions for the models of the G1S and G2S groups. The 326A model, which represents G1 group, works with a source function composed by a single wavelet, while in 330A and 330B models for G2 group, seven consecutive wavelets were used. These source functions suggest different energy release processes between LP earthquakes in the conduit (group G2) and LP events related to the formation of lava domes on the surface (group G1). It is therefore recommended for future research to delve into the details of these processes.

4.5. Other implications

Although there are several techniques to locate LP events that do not depend on the attenuation of seismic energy, it is common to use location methods based on the attenuation of seismic energy as a function of source-station distances (Kumagai et al., 2010; Torres, 2010; Torres and Cadena, 2009; Battaglia and Aki, 2003). In these techniques it is assumed that it is possible to use any wave train since the source-station distance is the same, but as we demonstrated in this study, there are different wave trains associated with different source points along the length of the conduit (i.e. the small pressure transient zone at the top and the bottom of the conduit), which implies that the distances traveled by the wave trains are different. It is possible that the precision of seismic location based on the attenuation of seismic energy can be improved considering the results of this study.

Finally, the distinction of wave trains in actual LP seismograms, the knowledge of their associated processes, the estimation of the length of the magma column, as well as the possibility of synthesizing seismograms with representative models of the associated processes, mean that this study could support the monitoring of volcanic activity.

5. Conclusions

During the 2004–2010 GV activity, LP seismicity was controlled by the presence of a magma column that gave rise to two LP groups with different waveforms and spectral content. These groups were related to the presence of lava domes on the surface (group G1) and magma that remained at depth below the conduit top (group G2).

Using synthetic models with magma filled conduits, we are able to recreate general characteristics of the waveforms and spectral content of LP events for G1 and G2 groups.

The length of the magma column and the source frequency control the differences between the models for synthetic earthquakes in the G1S and G2S groups.

The G1 group of seismicity is modeled using a 2800 m magma column length, with the top about 150 m from the surface and an energy release point located near the base of the conduit. The seismic source is represented by a series of pressure oscillations with a total duration of approximately 1.9 s approximately and a dominant frequency of 5 Hz. In contrast the seismicity of the G2 group was related to a shorter magma column, 1960 m in length, whose top is about 1000 m from the surface. Our work suggest that these waveforms were excited by a point source close to the conduit base and were made up of a single pressure oscillation with a dominant frequency of 8 or 10 Hz and a duration of less than 0.3 s.

In the future this research should be extended to Galeras activity from 1989 through 1993, since the characteristics of that activity are similar to the 2004–2010 activity period, especially during the lava dome emplacement at 1991.

CRediT authorship contribution statement

Óscar E. Cadena: Conceptualization, Methodology, Software, Formal analysis, Investigation, Data curation, Writing - original draft, Visualization, Project administration, Funding acquisition. **John J. Sánchez:** Validation, Investigation, Resources, Writing - review & editing, Visualization, Supervision.

Declaration of competing interest

The authors declare that they have no known competing financial interests or personal relationships that could have appeared to influence the work reported in this paper.

document.

Appendix A. Supplementary data

Supplementary data to this article can be found online at https://doi.org/10.1016/j.jsames.2021.103661.

References

Bain, et al., 2019. Textural and geochemical constraints on andesitic plug emplacement prior to the 2004 – 2010 vulcanian explosions at Galeras volcano, Colombia. J. Volcanol. Geoth. Res. https://doi.org/10.1016/j.jvolgeores.2019.05.001 0377-0273.

Battaglia, J., Aki, K., 2003. Location of seismic events and eruptive fissures on the Piton de la Fournaise volcano using seismic amplitudes. J. Geophys. Res. https://doi.org/10.1029/2002JB002193.

Brocher, T., 2005. Earthquake Hazard Assessment of Southern California View Project Yucca Mountain Project View Project Empirical Relations between Elastic Wavespeeds and Density in the Earth's Crust. Bulletin of the Seismological Society of America. https://doi.org/10.1785/0120050077.

Cadena, O., 2021. Modelos de fuente de sismicidad LP para la actividad del volcán Galeras 2004-2010 (Colombia). Universidad Nacional de Colombia. Tesis doctoral.

Calvache, M., 1990. Geology and Vulcanology of the Recent Evolution of the Galeras Volcano, Colombia. Ms. Thesis. Louisiana State University.

Calvache, V.M.L., Williams, S.N., 1997. Emplacement and petrological evolution of the andesitic dome of Galeras volcano, 1990–1992. J. Volcanol. Geoth. Res. https://doi.org/10.1016/S0377-0273(96)00086-8.

Campagnola, S., Romano, C., Mastin, L.G., Vona, A., 2016. Confort 15 model of conduit dynamics: applications to Pantelleria Green Tuff and Etna 122 BC eruptions. Contrib. Mineral. Petrol. 171 (6) https://doi.org/10.1007/s00410-016-1265-5.

Carcolé, E., Ugalde, A., Vargas, C.A., 2006. Three-dimensional spatial distribution of scatterers in Galeras volcano, Colombia. Geophys. Res. Lett. 33 (8) https://doi.org/10.1029/2006GL025751.

Cepeda, H., 2020. Quinientos años de documentación histórica de actividad del volcán Galeras: escenarios eruptivos. Servicio Geológico Colombiano.

Chouet, B., 1986. Dynamics of a fluid-driven crack in three dimensions by the finite difference method. J. Geophys. Res. 91 (B14), 13967. https://doi.org/10.1029/jb091ib14p13967.

Chouet, B., 1988. Resonance of a fluid-driven crack: radiation properties and implications for the source of long-period events and harmonic tremor. J. Geophys. Res. 93 (B5), 4375–4400. https://doi.org/10.1029/JB093iB05p04375.

Clay, C., Medwin, H., Wiley and Sons, J., 1977. Acoustical oceanography: principles and applications. J. Sound Vib. https://doi.org/10.1016/S0022-460X(78)80104-7. New York.

Collier, L., Neuberg, J., 2006. Incorporating seismic observations into 2D conduit flow modeling. J. Volcanol. Geoth. Res. 152 (2006), 331–346.

COMSOL Multiphysics Reference Manual, 2019. www.comsol.com.

Espinosa, A., 2001. Erupciones históricas de los volcanes colombianos (1500-1995). Editorial Guadalupe Ltda. Bogotá.

Ferrazzini, V., Aki, K., 1987. Slow waves trapped in a fluid-filled infinite crack: implication for volcanic tremor. J. Geophys. Res. 92 (B9), 9215. https://doi.org/10.1029/jb092ib09p09215.

Goff, F., Stimac, J., Larocque, A., Jr, P.T., 1994. Gold degassing and deposition. GSA Today from. https://www.geosociety.org/gsatoday/archive/4/10/pdf/i1052-5173-4-10-sci.pdf.

Gómez, D., Laverde, C., Mier, R., 2006. Aproximaciones metodológicas para el cálculo de volúmenes de domos de lava – caso de estudio volcán galeras (1991 – 2006). INGEOMINAS, Informe interno.

Harnett, C.E., Thomas, M.E., Purvance, M.D., Neuberg, J., 2018. Using a discrete element approach to model lava dome emplacement and collapse. J. Volcanol. Geoth. Res. 359, 68–77. https://doi.org/10.1016/j.jvolgeores.2018.06.017.

INGEOMINAS, 2006. Boletín semestral de actividad del volcán Galeras enero a junio de 2006. Pasto-Colombia, Informe público.

INGEOMINAS, 2008a. Boletín mensual de actividad del volcán Galeras enero de 2008. Pasto-Colombia, Informe público.

INGEOMINAS, 2008b. Boletín semestral de actividad del volcán Galeras enero a junio de 2008. Pasto-Colombia, Informe público.

INGEOMINAS, 2008c. Informe de resultados, análisis de oxidos mayores muestra roca volcán Galeras. Laboratorio de Geoquímica INGEOMINAS, Bogotá-Colombia.

Jousset, P., Neuberg, J., Sturton, S., 2003. Modelling the time-dependent frequency content of low-frequency volcanic earthquakes. J. Volcanol. Geoth. Res. 128 (1–3), 201–223. https://doi.org/10.1016/S0377-0273(03)00255-5.

Jousset, P., Neuberg, J., Jolly, A., 2004. Modelling low-frequency volcanic earthquakes in a viscoelastic medium with topography. J. Volcanol. Geoth. Res.

Julian, B.R., 1994. Volcanic tremor: nonlinear excitation by fluid flow. J. Geophys. Res. 99 (B6) https://doi.org/10.1029/93jb03129.

Kumagai, H., Nakano, M., Maeda, T., Yepes, H., Palacios, P., Ruiz, M., Arrais, S., Vaca, M., Molina, I., Yamashima, T., 2010. Broadband seismic monitoring of active volcanoes using deterministic and stochastic approaches. J. Geophys. Res. https://doi.org/10.1029/2009JB006889.

Londoño, J.M., Ospina, M.F., 2008. Estructura tridimensional de velocidad de onda P para el volcán Galeras. Bol. Geol. - Ingeominas 42 (1–2), 7–24.

Mastin, L.G., 2002. Insights into volcanic conduit flow from an open-source numerical model. G-cubed 3 (7).

Moncayo, E., 2004. Tomografía por coda Q en el volcán Galeras Nariño. Thesis de pregrado. Universidad Nacional de Colombia. https://doi.org/10.1016/j.jvolgeores.2007.07.019.

Murcia, L., Cepeda, H., 1991. Mapa Geológico de Colombia, Plancha 410, La Unión, Memoria explicativa. INGEOMINAS.

Neuberg, J., Luckett, R., Baptie, B., Olsen, K., 2000. Models of tremor and low-frequency earthquake swarms on Montserrat. J. Volcanol. Geoth. Res. 101 (1–2), 83–104. https://doi.org/10.1016/S0377-0273(00)00169-4.

Neuberg, J.W., Tuffen, H., Collier, L., Green, D., Powell, T., Dingwell, D., 2006. The trigger mechanism of low-frequency earthquakes on Montserrat. J. Volcanol. Geoth. Res. 153 (1–2 SPEC. ISS.), 37–50. https://doi.org/10.1016/j.jvolgeores.2005.08.008.

Ortega, A., 2014. Modelo de fuentes de anomalías gravimétricas regional y locales del volcán Galeras, asociadas a su estado de actividad entre junio 2008 – abril de 2009. Universidad Nacional de Colombia. http://www.bdigital.unal.edu.co/12895.

Pulgarín, B., 2006. Informe del apoyo en las labores geológicas del volcán Galeras en el periodo del 13 al 17 de junio de 2006 (Erupción del 12 de julio de 2006). INGEOMINAS, Informe interno.

Sanchez, J., Gomez, D., Torres, R., Calvache, M., Ortega, A., Ponce, P., Acevedo, A., Gil, F., Londoño, J., Rodriguez, S., Patiño, J., Bohórquez, O., 2005. Spatial mapping of the b-value at Galeras volcano, Colombia, using earthquakes recorded from 1995 to 2002. Earth Sci. Res. J. 9 (1), 30–66.

Smith, P., 2006. Combining Magma Flow Models with Seismic Signals. Msc. Thesis. School of Earth and Enviroment The University of Leeds.

Stix, J., Zapata, J., Calvache, M., Cortés, G., Fischer, T., Gómez, D., Narváez, L., Ordoñez, M., Ortega, A., Torres, R., Williams, S., 1993. A model of degassing at Galeras Volcano, Colombia, 1988-1993. October 2009, 1988–1993. Geol. Soc. America 21, 963–967. https://doi.org/10.1130/0091-7613(1993)021<0963.

Stix, J., Zapata, J., Calvache, M., Cortés, G., Fischer, T., Gómez, D., Narváez, L., Ordoñez, M., Ortega, A., Torres, R., Williams, S., 1997. A model of vulcanian eruptions at Galeras volcano, Colombia, 77. The Geological Society of America, pp. 285–303.

Sturton, S., Neuberg, J., 2003. The effects of a decompression on seismic parameter profiles in a gas-charged magma. J. Volcanol. Geoth. Res. 128 (1–3), 187–199. https://doi.org/10.1016/S0377-0273(03)00254-3.

Sturton, S., Neuberg, J., 2006. The effects of conduit length and acoustic velocity on conduit resonance: implications for low-frequency events. J. Volcanol. Geoth. Res. 151 (4), 319–339. https://doi.org/10.1016/j.jvolgeores.2005.09.009.

Torres, R., 2010. Locating Long Period Events and Tremor beneath Galeras Volcano Using Seismic Amplitudes – Stochastic Approach. M.S. thesis Building Research Institute, Tokyo-Japan.

Torres, R., 2012. Modelo 3D del volcán Galeras utilizando tomografía sísmica. Universidad Nacional de Colombia. http://bdigital.unal.edu.co/9836/.

Torres, R., Cadena, O., 2009. Cálculo de hipocentros para sismos volcánicos asociados al movimiento de fluidos en el volcán Galeras, Colombia, vol. 8. Universidad pedagógica y Tecnológica de Colombia (UPTC). N° 1.

Vargas, C.A., Duran, J.P., Pujades, L.G., 2006. Coda Q Tomography at the Galeras Volcano, Colombia. Universidad Nacional de Colombia. Departamento de Geociencias.